Research Article | Vol. 26, No. 9 | 30 Apr 2018 | OPTICS EXPRESS 11877
Optics EXPRESS

Optical constants modelling in silicon nitride membrane transiently excited by EUV radiation

R. Mincigrucci,[1,2,3] D. Naumenko,[1,2,4] L. Foglia,[1] I. Nikolov,[1] E. Pedersoli,[1] E. Principi,[1] A. Simoncig,[1] M. Kiskinova,[1] C. Masciovecchio,[1] F. Bencivenga,[1] and F. Capotondi[1]

[1]*Elettra Sincrotrone Trieste ScPA, Strada Statale 14 - km 163, 5 in AREA Science Park, Trieste, Italy*
[2]*Authors contributed equally*
[3]*riccardo.mincigrucci@elettra.eu*
[4]*denys.naumenko@elettra.eu*

Abstract: We hereby report on a set of transient optical reflectivity and transmissivity measurements performed on silicon nitride thin membranes excited by extreme ultraviolet (EUV) radiation from a free electron laser (FEL). Experimental data were acquired as a function of the membrane thickness, FEL fluence and probe polarization. The time dependence of the refractive index, retrieved using Jones matrix formalism, encodes the dynamics of electron and lattice excitation following the FEL interaction. The observed dynamics are interpreted in the framework of a two temperature model, which permits to extract the relevant time scales and magnitudes of the processes. We also found that in order to explain the experimental data thermo-optical effects and inter-band filling must be phenomenologically added to the model.

OCIS codes: (120.4530) Optical constants; (120.6810) Thermal effects; (140.7240) UV, EUV, and X-ray lasers; (140.7300) Visible lasers.

References and links

1. T. T. Yeh, H. Shirai, C. M. Tu, T. Fuji, T. Kobayashi, and C. W. Luo, "Ultrafast carrier dynamics in Ge by ultra-broadband mid-infrared probe spectroscopy," Sci. Rep. **7**, 40492 (2017).
2. I. Hamberg, C. G. Granqvist, K. F. Berggren, B. E. Sernelius, and L. Engström, "Band-gap widening in heavily Sn-doped In2O3," Phys. Rev. B **30(6)**, 3240–3249 (1984).
3. E. Allaria, R. Appio, L. Badano, W. Barletta, S. Bassanese, S. Biedron, A. Borga, E. Busetto, D. Castronovo, P. Cinquegrana, S. Cleva, D. Cocco, M. Cornacchia, P. Craievich, I. Cudin, G. D'Auria, M. Dal Forno, M. Danailov, R. De Monte, G. De Ninno, P. Delgiusto, A. Demidovich, S. Di Mitri, B. Diviacco, A. Fabris, R. Fabris, W. Fawley, M. Ferianis, E. Ferrari, S. Ferry, L. Froehlich, P. Furlan, G. Gaio, F. Gelmetti, L. Giannessi, M. Giannini, R. Gobessi, R. Ivanov, E. Karantzoulis, M. Lonza, A. Lutman, B. Mahieu, M. Milloch, S. Milton, M. Musardo, I. Nikolov, S. Noe, F. Parmigiani, G. Penco, M. Petronio, L. Pivetta, M. Predonzani, F. Rossi, L. Rumiz, A. Salom, C. Scafuri, C. Serpico, P. Sigalotti, S. Spampinati, C. Spezzani, M. Svandrlik, C. Svetina, S. Tazzari, M. Trovo, R. Umer, A. Vascotto, M. Veronese, R. Visintini, M. Zaccaria, D. Zangrando, and M. Zangrando, "Highly coherent and stable pulses from the FERMI seeded free-electron laser in the extreme ultraviolet," Nat. Photonics **6**, 699–704 (2012).
4. C. Grazioli, C. Callegari, A. Ciavardini, M. Coreno, F. Frassetto, D. Gauthier, D. Golob, R. Ivanov, B. Mahieu, B. Bučar, M. Merhar, P. Miotti, L. Poletto, E. Polo, B. Ressel, C. Spezzani, and G. De Ninno, "CITIUS: An infrared-extreme ultraviolet light source for fundamental and applied ultrafast science," Rev. Sci. Instrum. **85(2)**, 023104 (2014).
5. B. Frietsch, R. Carley, K. Döbrich, C. Gahl, M. Teichmann, O. Schwarzkopf, P. Wernet, and M. Weinelt, "A high-order harmonic generation apparatus for time- and angle-resolved photoelectron spectroscopy," Rev. Sci. Instrum. **84(7)**, 075106 (2013).
6. "SwissFEL https://www.psi.ch/swissfel/," .
7. "XFEL https://www.xfel.eu/," .
8. "LCLS https://lcls.slac.stanford.edu/," .
9. F. Bencivenga, R. Cucini, F. Capotondi, A. Battistoni, R. Mincigrucci, E. Giangrisostomi, A. Gessini, M. Manfredda, I. P. Nikolov, E. Pedersoli, E. Principi, C. Svetina, P. Parisse, F. Casolari, M. B. Danailov, M. Kiskinova, and C. Masciovecchio, "Four-wave mixing experiments with extreme ultraviolet transient gratings," Nature. **520**, 205–208 (2015).
10. F. Casolari, F. Bencivenga, F. Capotondi, E. Giangrisostomi, M. Manfredda, R. Mincigrucci, E. Pedersoli, E. Principi, C. Masciovecchio, and M. Kiskinova, "Role of multilayer-like interference effects on the transient optical response of

#323269 https://doi.org/10.1364/OE.26.011877
Journal © 2018 Received 16 Feb 2018; accepted 26 Mar 2018; published 24 Apr 2018

Optics EXPRESS

Si3N4 films pumped with free-electron laser pulses," Appl. Phys. Lett. **104(19)**, 191104 (2014).
11. S. Eckert, M. Beye, A. Pietzsch, W. Quevedo, M. Hantschmann, M. Ochmann, M. Ross, M. P. Minitti, J. J. Turner, S. P. Moeller, W. F. Schlotter, G. L. Dakovski, M. Khalil, N. Huse, and A. Föhlisch, "Principles of femtosecond X-ray/optical cross-correlation with X-ray induced transient optical reflectivity in solids," Appl. Phys. Lett. **106**, 061104 (2015).
12. F. Capotondi, E. Pedersoli, N. Mahne, R. H. Menk, G. Passos, L. Raimondi, C. Svetina, G. Sandrin, M. Zangrando, M. Kiskinova, S. Bajt, M. Barthelmess, H. Fleckenstein, H. N. Chapman, J. Schulz, J. Bach, R. Frömter, S. Schleitzer, L. Müller, C. Gutt, and G. Grübel, "Invited Article: Coherent imaging using seeded free-electron laser pulses with variable polarization: First results and research opportunities," Rev. Sci. Instrum. **84(5)**, 051301 (2013).
13. F. Capotondi, E. Pedersoli, F. Bencivenga, M. Manfredda, N. Mahne, L. Raimondi, C. Svetina, M. Zangrando, A. Demidovich, I. Nikolov, M. Danailov, and C. Masciovecchio, "free-electron lasers Multipurpose end-station for coherent diffraction imaging and scattering at FERMI @ Elettra free-electron laser facility free-electron lasers," J. Synchrotron Radiat. **22**, 544–552 (2015).
14. M. Danailov, F. Bencivenga, F. Capotondi, F. Casolari, P. Cinquegrana, A. Demidovich, E. Giangrisostomi, M. Kiskinova, G. Kurdi, M. Manfredda, C. Masciovecchio, R. Mincigrucci, I. Nikolov, E. Pedersoli, E. Principi, and P. Sigalotti, "Towards jitter-free pump-probe measurements at seeded free electron laser facilities," Opt. Express **22(11)**, 12869–12879 (2014).
15. J. Daillant and A. Gibaud, *X-Ray and Neutron Reflectivity: Principles and Applications*, Lecture Notes in Physics Monographs (Springer Berlin Heidelberg, 2003).
16. H. Fujiwara, *Spectroscopic Ellipsometry: Principles and Applications* (Wiley, 2007).
17. M. Born, E. Wolf, and A. B. Bhatia, *Principles of Optics: Electromagnetic Theory of Propagation, Interference and Diffraction of Light* (Cambridge University Press, 1999).
18. R. Jacobsson, "Light reflection from films of continuously varying refractive index," Prog. Opt. **5**, 247–286 (1966).
19. "CXRO http://www.cxro.lbl.gov/," .
20. H. G. Tompkins and E. A. Irene, eds., *Handbook of Ellipsometry* (Springer, 2005).
21. W. S. Fann, R. Storz, H. W. Tom, and J. Bokor, "Electron thermalization in gold," Phys. Rev. B **46(20)**, 13592–13595 (1992).
22. B. H. Christensen, K. Vestentoft, and P. Balling, "Short-pulse ablation rates and the two-temperature model," Appl. Surf. Sci. **253(15)**, 6347–6352 (2007).
23. A. Rämer, O. Osmani, and B. Rethfeld, "Laser damage in silicon: Energy absorption, relaxation, and transport," J. Appl. Phys. **116(5)**, 053508 (2014).
24. T. Shin, S. W. Teitelbaum, J. Wolfson, M. Kandyla, and K. A. Nelson, "Extended two-temperature model for ultrafast thermal response of band gap materials upon impulsive optical excitation," J. Chem. Phys. **143(19)**, 194705 (2015).
25. P. Jonnard, Jean-Michel André, K. L. Guen, M. Wu, E. Principi, A. Simoncig, A. Gessini, R. Mincigrucci, C. Masciovecchio, and O. Peyrusse, "EUV stimulated emission from MgO pumped by FEL pulses," Struct. Dyn. **4(5)**, 054306 (2017).
26. R. Lam, S. Raj, T. Pascal, C. Pemmaraju, L. Foglia, A. Simoncig, N. Fabris, P. Miotti, C. Hull, A. Rizzuto, J. Smith, R. Mincigrucci, C. Masciovecchio, A. Gessini, E. Allaria, G. De Ninno, B. Diviacco, E. Roussel, S. Spampinati, G. Penco, S. Di Mitri, M. Trovò, M. Danailov, S. Christensen, D. Sokaras, T.-C. Weng, M. Coreno, L. Poletto, W. Drisdell, D. Prendergast, L. Giannessi, E. Principi, D. Nordlund, R. Saykally, and C. Schwartz, "Soft X-ray second harmonic generation as an interfacial probe," Phys. Rev. Lett. **120(2)**, 023901 (2018).
27. A. Calvi, "Refractive index changes induced by EUV transient grating," In preparation (2018).
28. N. Medvedev and B. Rethfeld, "Transient dynamics of the electronic subsystem of semiconductors irradiated with an ultrashort vacuum ultraviolet laser pulse," New J. Phys. **12**, 073037 (2010).
29. M. Breusing, C. Ropers, and T. Elsaesser, "Ultrafast carrier dynamics in graphite," Phys. Rev. Lett. **102(8)**, 086809 (2009).
30. W. H. Press, *Numerical Recipes 3rd Edition: The Art of Scientific Computing* (Cambridge University Press, 2007).
31. A. V. Shaposhnikov, I. P. Petrov, V. A. Gritsenko, and C. W. Kim, "Electronic band structure and effective masses of electrons and holes in the α and β phases of silicon nitride," Phys. Solid State **49(9)**, 1628–1632 (2007).
32. S. M. Durbin, "X-ray induced optical reflectivity," AIP Adv. **2(4)**, 042151 (2012).
33. A. Arbabi and L. L. Goddard, "Measurements of the refractive indices and thermo-optic coefficients of Si3N4 and SiO(x) using microring resonances." Opt. Lett. **38(19)**, 3878–3881 (2013).
34. N. Medvedev, Z. Li, and B. Ziaja, "Thermal and nonthermal melting of silicon under femtosecond x-ray irradiation," Phys. Rev. B **91(5)**, 054113 (2015).
35. V. Tkachenko, N. Medvedev, Z. Li, P. Piekarz, and B. Ziaja, "Transient optical properties of semiconductors under femtosecond X-ray irradiation," Phys. Rev. B **93(14)**, 144101 (2016).

1. Introduction

Pump-probe techniques are routinely employed in laser laboratories to conduct studies in a number of scientific fields. Generally, transient reflectivity measurements are more sensitive to the electron dynamics, while transient absorption data are more responsive to the activated

Optics EXPRESS

absorption mechanism [1, 2]. However, the pump-probe techniques in the paEq.st were confined in the infrared (IR) to ultraviolet (UV) spectral region. The advent of high harmonic generation sources and recent FEL facilities has enabled expanding these techniques in the EUV [3–6] and x-rays range [7, 8]. Pump-probe measurements are also routinely employed at FEL facilities as a diagnostic tool to achieve temporal superposition between FEL and optical pulses or to synchronize two or more FEL pulses for more complex experiments [9]. Silicon nitride (Si_3N_4) posseses a number of interesting features as a material for microelectronics: it is chemically inert, resistant to high temperatures (melting point is located at ~2100° K) and with a wide band gap ($E_g \sim 4.5$ eV) making it transparent in the visible range. Recent advances in chemical vapour deposition techniques have enabled the realization of robust Si_3N_4 thin films, employed as x-ray and electron transparent windows in environmental cells used in microscopy. Si_3N_4 transient electronic properties after an EUV/x-ray excitation have been studied and widely employed at FEL facilities for timing diagnostics.

Different studies have been carried out to characterize FEL induced transient reflectivity of thin Si_3N_4 films. They evidenced, e.g., the role of the substrate [10] in interferential magnifying/weakening the signal and the advantages of operating close to Brewster angle to maximize the signal-to-noise ratio [11]. However, a simple interpretation which relates the values of the optical constants to the FEL intensity, wavelength and to the material parameters is still lacking. We hereby report a study performed at the Italian FEL, FERMI, on transient optical response of Si_3N_4 sample as a function of its thickness, FEL fluence and probe polarization.

2. Experimental

The experiment was performed at the DiProI end station [12, 13] on three Si_3N_4 membranes of nominal thickness 50, 100 and 500 nm. The samples, mounted inside the DiProI chamber, were excited by FEL pulses with 25 nm wavelength and 50 fs pulse duration, focused to 150x150 μm^2 by Kirkpatrick-Baez bendable mirrors. We used three different FEL fluences: I_f = 13, 7, and 4 mJ/cm^2 and no sample damage was observed even at the highest fluence. The excited region of the sample was probed by an intrinsically synchronized with the FEL emission optical pulse (780 nm wavelength) [14], impinging onto the sample at 45 degrees (see Fig. 1).

The probe pulse had a spot size of about 100 μm full width half maximum, an energy of 1.2 μJ and a time duration of about 100 fs. The polarizer, sketched in Fig. 1, was a half wave plate that allows fast switch between s- and p-polarization with motorized rotator. The transmitted and reflected intensities were detected by two nominally identical Basler Scout cameras. The recorded experimental traces are reported in Figs. 2-3.

3. Results and discussion

Experimental data from three samples of different thicknesses were collected using the three FEL fluences and both polarizations. We made use of x-ray reflectivity (XRR) to measure the thicknesses of the membranes [15] that provided the values of 38±2 nm, 110±6 nm and 630±60 nm as we show in Appendix 5.1 (Fig. 6). However, for the thickest membrane interferential effects play an important role in reflection geometry, degrading the XRR measurements. To better reproduce the experimental traces its thickness has also been evaluated to the data, resulting in a value of 575 nm. The measured values were employed for the other two membranes, i.e. 38 and 110 nm. In this section we show only transient reflectivity ($\Delta R/R$) and transmissivity ($\Delta T/T$) data for s-polarized light. The dataset, employed in the optical constants retrieval, is reported in Appendix 5.2 (Fig. 7). The traces are characterized by a sharp initial drop, as a function of I_f (Fig. 2), mainly dominated by the cross-correlation of the input pulses, followed by a fast recovery (~ 1 ps) culminating in a plateau. The latter is well appreciable at the highest I_f while it is barely visible at the lowest flux, where the reflectivity regains the nominal value. The magnitude of the

Optics EXPRESS

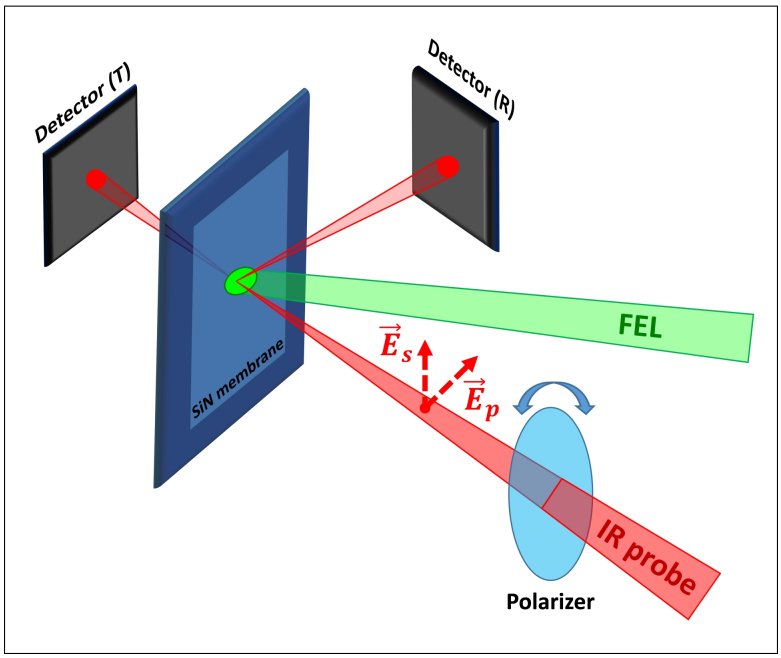

Fig. 1. Sketch of the experimental set-up.

sharp peak in the $\Delta R/R$ traces linearly scales with I_f passing from $\sim 8\%$ at 13 mJ/cm^2 to $\sim 3\%$ at 4 mJ/cm^2.

The data collected at the highest I_f as function of the membrane thickness are shown in Fig. 3. Also in this case, the traces are characterized by an initial drop followed by a plateau. However, while the initial drop is always negative, the plateau changes from positive values (38 nm case) to negative ones (575 nm case). $\Delta T/T$ traces (see also Appendix 5.2, Fig. 7) are always characterized by an initial drop, driven by the pulse cross correlation, followed by a partial recovery. As for the $\Delta R/R$ traces, the drop amplitude scales almost linearly with the fluence. The physical phenomena giving rise to the observed signals have to be the same irrespectively of the membrane thicknesses and I_f. This suggests that the interference between the excited portion of the sample and the substrate, combined with the exponential decay of the excitation into the sample have to be carefully treated for correct description of the ongoing processes.

3.1. Optical constants retrieval

We used the Jones matrix formalism to mathematically simulate the changes undergone by the initial field amplitudes E_i to the amplitudes resulting from the interaction with the sample, both in reflection (E_r) and in transmission (E_t) geometry [16]. We represented the FEL excited Si_3N_4 membrane as a multilayer structure [17, 18], where the refractive index n and the extinction coefficient k exponentially decay in the direction of the FEL pulse propagation (z-axis). We model the system as 1 nm thick homogeneous layers. The decay constant α was calculated from the EUV attenuation length in Si_3N_4, and its value is $\alpha = 0.026$ nm^{-1} [19]. The amplitudes resulting from the interaction with the sample are given by [16, 20]:

$$\begin{pmatrix} E_p^{r(t)} \\ E_s^{r(t)} \end{pmatrix} = \begin{pmatrix} r_p(t_p) & 0 \\ 0 & r_s(t_s) \end{pmatrix} \begin{pmatrix} E_p^i \\ E_s^i \end{pmatrix} \tag{1}$$

Optics EXPRESS

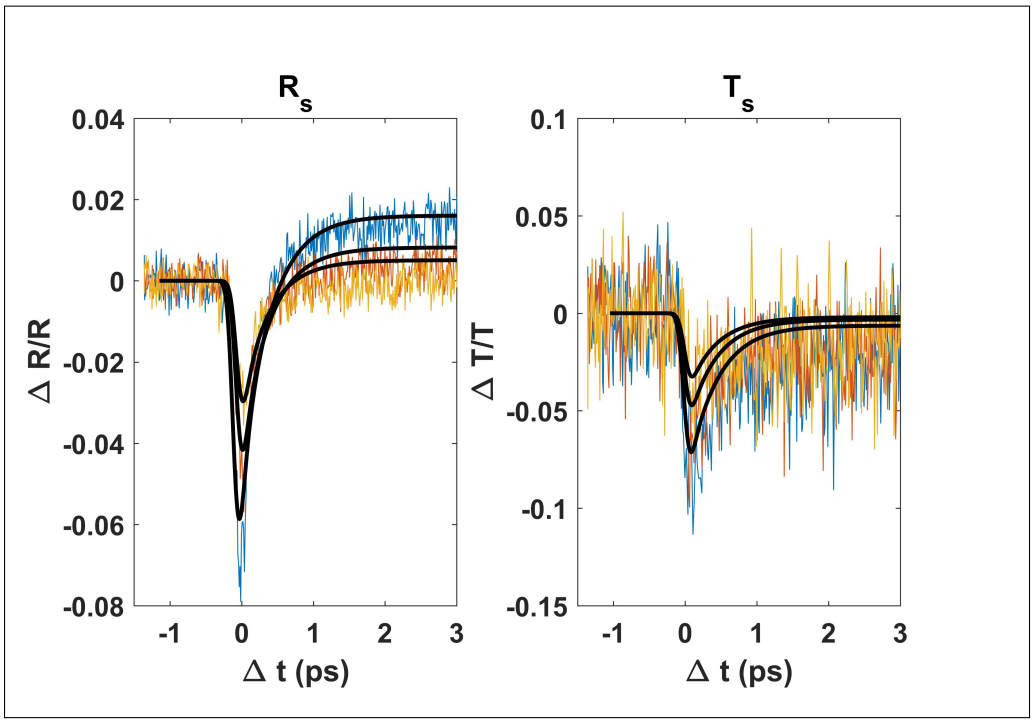

Fig. 2. Transient reflectivity (left panel) and transmissivity (right panel) traces for s-polarized light measured on the thinnest (38 nm) Si_3N_4 membrane as function of the FEL fluence. Blue, red and yellow traces were recorded at 13, 7 and 4 mJ/cm^2, respectively. Thick lines are the calculated profiles. See text for further details.

where r_s, r_p, t_s, t_p are total amplitude reflection and transmission coefficients for the whole multilayer structure.

They include interference effects and are given by recursive formula:

$$\widetilde{r}^k_{p(s)} = \frac{r^k_{p(s)} + \widetilde{r}^{k+1}_{p(s)} e^{-2i\beta_k}}{1 + r^k_{p(s)} \widetilde{r}^{k+1}_{p(s)} e^{-2i\beta_k}}, \widetilde{t}_{p(s)} = \frac{t^k_{p(s)} \widetilde{t}^{k+1}_{p(s)} e^{-i\beta_k}}{1 + r^k_{p(s)} \widetilde{r}^{k+1}_{p(s)} e^{-2i\beta_k}} \tag{2}$$

where β_k is the phase variation in the kth layer, $r^k_{p(s)}$ and $t^k_{p(s)}$ are the usual Fresnel coefficients at kth interface, while $\widetilde{r}^k_{p(s)}$ and $\widetilde{t}^k_{p(s)}$ are taking into account a wave propogation along the multilayer structure underneath the kth interface. The calculations are performed upward from the last membrane/vacuum interface where $\widetilde{r}\left(\widetilde{t}\right)^{k+1}_{p(s)} = r\left(t\right)^{k+1}_{p(s)}$. Finally, the total amplitude coefficients in 1 are given by $r\left(t\right)_{p(s)} = \widetilde{r}\left(\widetilde{t}\right)^{1}_{p(s)}$ [16]. Given the coefficient definitions and the exponential decay law for n and k, it is possible to derive four independent equations from 1, which allow a full retrieval of the excited optical constants. More details about the procedure can be also found in [10]. Following the Jones matrix inversion, it is possible to retrieve from the experimental data the values of the excited optical constants which are displayed in Fig.s 4-5; traces always refer to the first layer of the excited sample. The dependence of n is characterized by a small decrease close to the zero delay time value, followed by a sharp increase culminating in a plateau which is $\sim 1.5\%$ higher than the unperturbed value. Instead, the trend of k is characterized by an exponential like relaxation ($\tau \sim 0.6$ ps) after a ~ 0.1 ps rise, the latter being ascribable to the pulses cross-correlation.

Optics EXPRESS

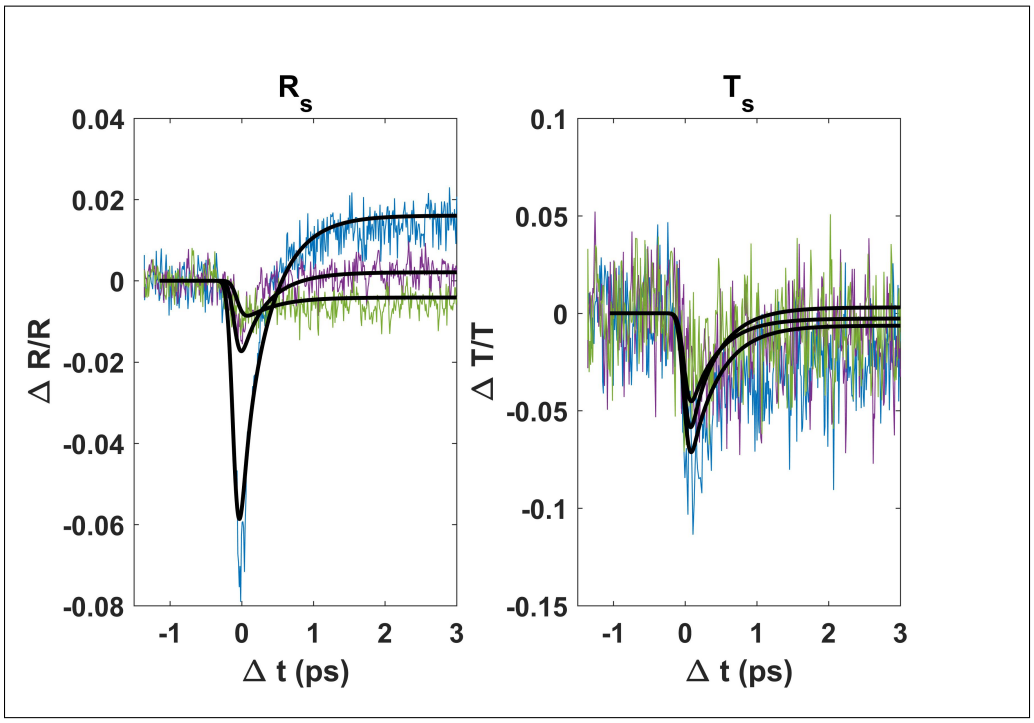

Fig. 3. Transient reflectivity (left panel) and transmissivity (right panel) traces for s-polarized light at 13 mJ/cm^2 FEL fluence as function of the sample thickness. Blue, purple and green traces are for 38, 110 and 575 nm thick membrane, respectively.

3.2. *Optical constants modelling*

The interaction of a short laser pulse with condensed matter can be described with the density dependent two temperature model (nTTM). This model was originally developed and applied to metals [21, 22] and subsequently extended to semicondutors [23, 24] to describe the thermal evolution of the electron and lattice systems. In the general case, the laser pulse is absorbed by the medium and and creates hot electrons but the presence of a bandgap in the semiconductors complicates the energy flow to the lattice due to electron-hole recombination events. The induced modifications of the free carrier density can have sensible effect on the ultrafast thermal evolution of band gap material [23]. In general, far from electronic core level absorption edges, free carrier absorption (FCA) is the most significant process describing the excitation of the material properties. It generates electron density variation close to the Drude plasma frequency for the optical probe. For the FEL case, the Drude equivalent electron density is about $4.5 * 10^{22}$ cm^{-3}, which is fairly larger than the one generated in the present case (see Eq. (4)); FCA for the FEL pulse (excitation process) was therefore neglected. Recent experimental findings [25, 26] have also shown that two photon effects have small cross sections. Thus the equation for the FEL propagation inside the material reduces to:

$$\frac{\partial I(z,t)}{\partial z} = -\alpha I(z,t) \tag{3}$$

i.e. the usual exponential attenuation. *A posteriori*, this strengthens the assumption of the exponential decay for the excitation profile made in Sec. 3.1.

Optics EXPRESS

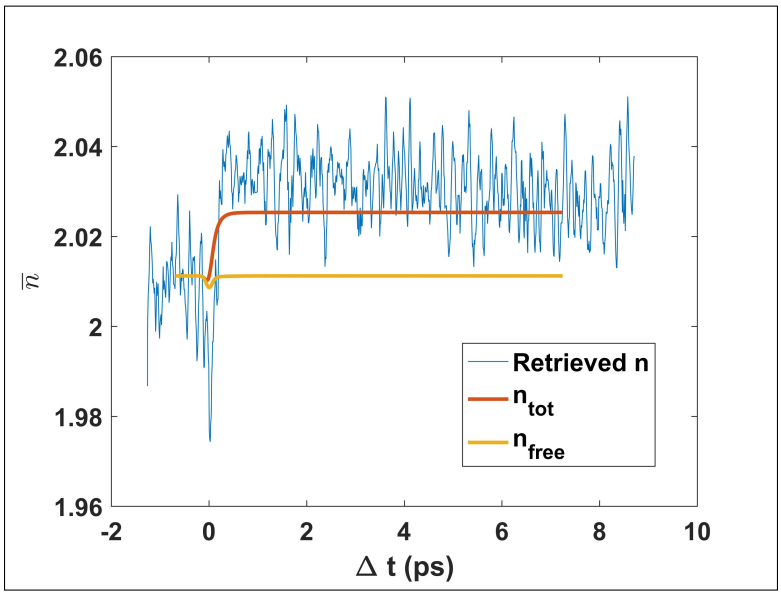

Fig. 4. Retrieved values for n (first layer of 38 nm thick membrane, blue trace) compared with the full modelization of n (red trace) and the free carriers contribution (yellow trace).

Electron (n_e) and hole (n_h) densities have been calculated using the equation derived from [23]:

$$\frac{\partial n_{e,(h)}(z,t)}{\partial t} = \frac{\alpha}{E_{ph}} I(z,t) - \gamma n_{e,(h)}(z,t)^3 + \left(\delta - \lambda_{e,(h)}\right) n_{e,(h)}(z,t) \tag{4}$$

where $E_{ph} = 50$ eV, $\gamma = 5 * 10^{-28} \frac{cm^6}{s}$ is the Auger rate [27], δ is the impact ionization coefficient and $\lambda_{e,(h)}$ are electron and hole losses. Losses coefficients may be understood as an effective parameter summarizing different phenomena which may take place into the material, as e.g. diffusion, eventually including the interface effects on it, photo-emission into vacuum and carrier recombination. Given the postulated linear dependence of the losses, it is straightforward to define the parameter $L_{e,(h)} = \delta - \lambda_{e,(h)}$ which can be obtained from the experimental data. A positive value for the L's coefficients indicates a preponderance of the impact ionization mechanism (charge generation). On the contrary, negative values mirror prevailing losses.

Electron temperatures (T_e) can be calculated according to:

$$C_e \frac{\partial T_e(z,t)}{\partial t} = \alpha I(z,t) - g\left(T_e - T_l\right) - \partial U\left(E_g, T_e, \frac{\partial n_e(z,t)}{\partial t}\right). \tag{5}$$

Here we also assume instantaneous thermalization of electrons and holes. The characteristic time for such process is estimated to be in the 10-30 fs time-scale [28,29], i.e. within our pulses duration. In such approximation, $C_e = 3 n_e k_b$ is the electron heat capacity, where k_b is the Boltzman constant; g is the carrier phonon coupling parameter given by $\frac{C_e}{\tau_{e-ph}}$, where τ_{e-ph} is the electron-phonon relaxation time and was evaluated through the data. Finally ∂U is the energy variation of the electron system defined as:

$$\partial U\left(E_g, T_e, \frac{\partial n_e(z,t)}{\partial t}\right) = \left(E_g + 3 k_b T_e\right) \frac{\partial n_e(z,t)}{\partial t} \tag{6}$$

where $E_g = 4.5$ eV is the electronic energy gap.

Optics EXPRESS

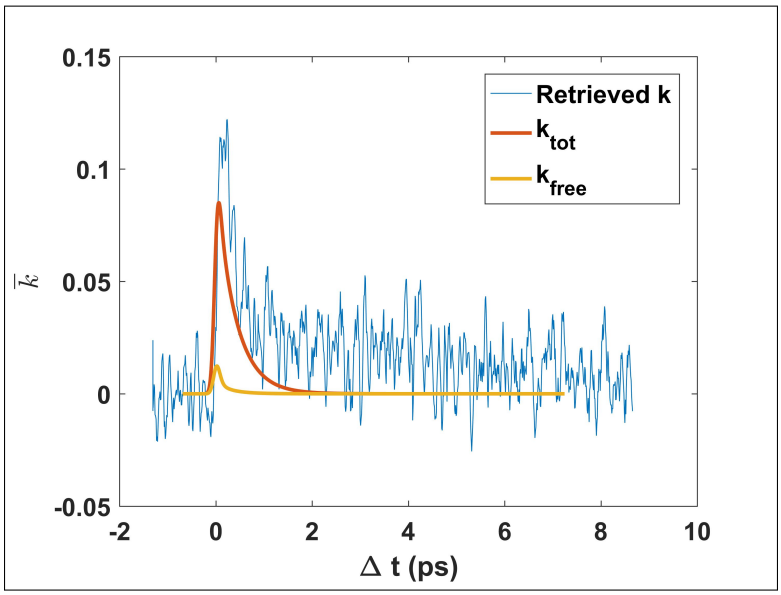

Fig. 5. Retrieved values for k (first layer of 38 nm thick membrane, blue trace) compared with the full modeling of k (red trace) and the free carriers contribution (yellow trace).

The lattice temperature (T_l) is defined through :

$$C_l \frac{\partial T_l(z,t)}{\partial t} = g\left(T_c - T_l\right), \tag{7}$$

where $C_l = 3.7 \frac{J}{Kcm^3}$ is the heat capacity. Equations (4), 5, 7 have been solved with a forward time Euler method [30], which enabled to determine the free carrier contribution to the dielectic function, using the Drude relation:

$$\epsilon(z,t) = \epsilon_r - D_e(z,t) - D_h(z,t) = \left(n_{free} + ik_{free}\right)^2 \tag{8}$$

$$D_{e(h)}(z,t) = \frac{n_{e(h)}(z,t)\, e^2}{\epsilon_0 m_{e(h)}} \frac{1}{\omega\left(\omega + i\nu(z,t)\right)} \tag{9}$$

where $\epsilon_r = 4.045$ is the relative dielectric permittivity (corresponding to $n_0 = 2.011$ for the IR probe), e is the electron charge, ϵ_0 is the vacuum permittivity, ω is the laser pulsation $2.41 * 10^{15}$ rad/s, $m_{e(h)}$ are the conduction effective masses, both equals to 0.5 electron masses [31], and $\nu(z,t)$ is the collisional frequency evaluated as:

$$\nu(z,t) = \frac{\sqrt{3}\epsilon_0 \pi \left(k_b T_c\right)^{1.5}}{2e^2} * \sqrt{\frac{1}{M_e} + \frac{1}{M_h}}. \tag{10}$$

In Eq. (10) $M_{e,h}$ are the density of states effective masses for electron and holes, corresponding to 0.3 and 3 electron masses, respectively [27]. The free carrier contributions to the optical constants may be easily calculated as $n_{free}(z,t) = \Re\left(\sqrt{\epsilon(z,t)}\right)$ and $k_{free}(z,t) = \Im\left(\sqrt{\epsilon(z,t)}\right)$. Carrier contributions represent ultra-fast system perturbations which may rapidly become irrelevant when the densities decrease below a value corresponding to a plasma frequency of the probe. In order to model the long time response, we took into account two slower processes; i.e. (i) dependence of n on T_l and (ii) the induced absorption due to partial valence band

Optics EXPRESS

depletion [32]. The former is generally accounted through the thermo-optic coefficient, while a precise quantification of the latter requires sophisticated calculations which make use of time dependent (TD) density functional theory (DFT). However, it is reasonable to assume that the photon absorption is proportional to the holes density. Provided probe photons further excite the valence electrons; this only pushes the holes to a higher energy level without altering their total number. Moreover, due to the continuity of the valence band the process can be considered to be always resonant, so the contribution to the dielectric function is purely imaginary and primarily affects the value of k. Following such reasoning the optical constants can be modelled as follow:

$$\begin{aligned} n(z,t) &= n_{free}(z,t) + ST_L(z,t) \\ k(z,t) &= k_{free}(z,t) + Zn_h(z,t) \end{aligned} \tag{11}$$

where S is the thermo-optic coefficient and Z is the proportionality coefficient between the induced absorption and the hole density. In summary, to model optical constants we modified the standard nTTM by introducing effective L's parameters that account for different phenomena (impact ionization, photo-emission, diffusion) that contribute to the carriers balance. A value of L_e different from L_h, e.g., may imply a sample charging. The thermo-optic effect, which alters the n value, has been phenomenologically included in the modelling through the lattice temperature while the inter-band absorption, affecting the k behavior, has been inserted assuming to be proportional to the holes density. The experimental data for reflectivity and transmissivity and the corresponding traces obtained with the nTTM calculations are shown in Appendix 5.2 (Fig. 7).

Fig. 4 displays a time evolution of the retrieved refractive index that shows a small initial dip followed by a sudden increase to a plateau. In the frame of our model, the initial drop, may be ascribed to rapid increase in the carrier densities which diminishes the n_0. We interpret the subsequent increase in term of the thermo-optic coefficient. The ultra-fast coupling transfers the energy from the carrier to the lattice subsystem, yielding to a status with a mean temperature (for the thinnest membrane) of ~900° K. This value has to be compared with the standard thermodynamic calculation which accounts for the total deposited energy $\left(\left(1-e^{-\alpha d}\right)E_0\right)$ into the sample volume divided by the mass and specific heat. Here d is the sample thickness. This value (900 °K), is in a good agreement with the nTTM calculations. Since the thermo-optic coefficient is positive, it is equivalent to an increase of the refractive index. An evaluation of the latter gives a value of $(15 \pm 5) * 10^{-5}$ 1/K for the S coefficient. This well compares to the one reported for Si_3N_4 at 1550 nm [33]. It is worth to stress that the sharp rise in n is not only determined by the electron phonon coupling parameter ($\tau_{e-ph} = 0.1 \pm 0.05$ ps), but rather by an interplay of the latter with the Auger recombination rate and the L's parameters. The evaluated values for these coefficients are: $L_e = (-10 \pm 1) * 10^{12}$ 1/s and $L_h = (-2.5 \pm 0.5) * 10^{12}$ 1/s. The negative sign suggests that the losses are higher and diffusion/photo-emission mechanisms can dominate the carrier dynamics. This scenario is also confirmed by an estimation of the diffusion coefficient, which may be conducted calculating the ratio between the time derivative and the Laplacian of the electron density. Close to the pulse peak the ratio between $\frac{\partial n_e(z,t)}{\partial t}$ and $\nabla^2 n_e(z,t)$ gives a value of ~ 1.1 cm^2/s which is of the same order of the ambipolar diffusion coefficient for Si at high temperatures (9 cm^2/s) [23].

The k trend (Fig. 5) is characterized by a sharp increase followed by an exponential-like decay. While FCA has been neglected for the FEL excitation process, it cannot be neglected for the optical probe. FCA contribution is relevant for the absolute value of the peak, while at longer delays (>0.5 ps) the shape and magnitude of the k coefficient are significantly influenced by induced absorption only. The evaluated value for Z is $(4 \pm 1) * 10^{-20}$ cm^3 and it can be compared with the one obtainable from the joint density of states (DOS). Though, the DOS of valence electrons and holes depends on the density, thus leading to a time and density dependent value for Z. However, in a hybrid and simple approach, this value can be obtained using DFT calculations

Optics EXPRESS

and plugged in Eq.(11) to reconstruct the experimental data.

The retrieved curves for the optical parameters show similar shapes for the three membranes (see Appendix 5.2, Fig. 8). However, at equal FEL fluxes, the magnitude of the transient reflectivity and transmissivity are quite different. This is due to the major role played by interferential effects. The latter evidence suggests that in EUV pump-optical probe experiments, where the excitation has a strong gradient along the pump propagation direction, a deeper understanding of the underlying physics is gained through optical constants modelling rather than through the direct parametrization of transient reflectivity/transmissivity.

4. Conclusion

In conclusion, we presented a campaign of pump-probe reflectivity and transmissivity measurements at 25 nm excitation wavelength, performed as a function of the pump fluence, sample thickness and probe polarization. Using Jones matrix formalism and the assumption of an excitation exponential decay, we retrieved the time dependent complex refractive index of the excited Si_3N_4 and a nTTM model was employed to interpret its behavior. We found that changes in the optical constants are not only due to free carriers contributions, but slower processes plays a significant role. The thermo-optic effect and induced absorption mechanisms have to be taken into account to reproduce the experimental data. Our approach permits to obtain information on sample dynamics in a simple and effective way, contrary to more sophisticated calculations [34, 35]. Due to the high number of involved parameters and to their strong interplay it is difficult to evaluate their contributions and define the precise values. However, some phenomena as impact ionization, photo-emission, diffusion and charge trapping can be in principle extracted and evaluated. In its present form all these effects are summarized in the L's parameters which offer an overview of the comprehensive balance.

5. Appendix

5.1. X-ray reflectivity data

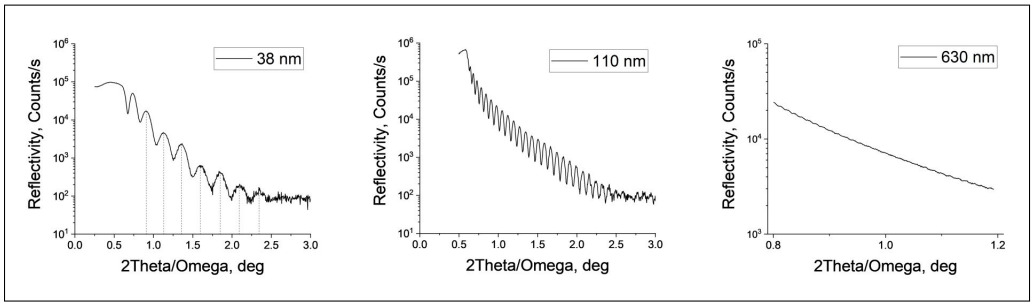

Fig. 6. XRR data (PanalyticalX'pert, λ = 0.15405 nm) for the three Si_3N_4 membranes. The calculated thicknesses using the X'pert Epitaxy software are 38±2 nm, 110±6 nm and 630±60 nm, respectively. Note that to reproduce the optical data the thickness of the thickest membrane was corrected to 575 nm (within a deviation of XRR measurements).

5.2. Dataset on optical constants retrieval and modelling

Optics EXPRESS

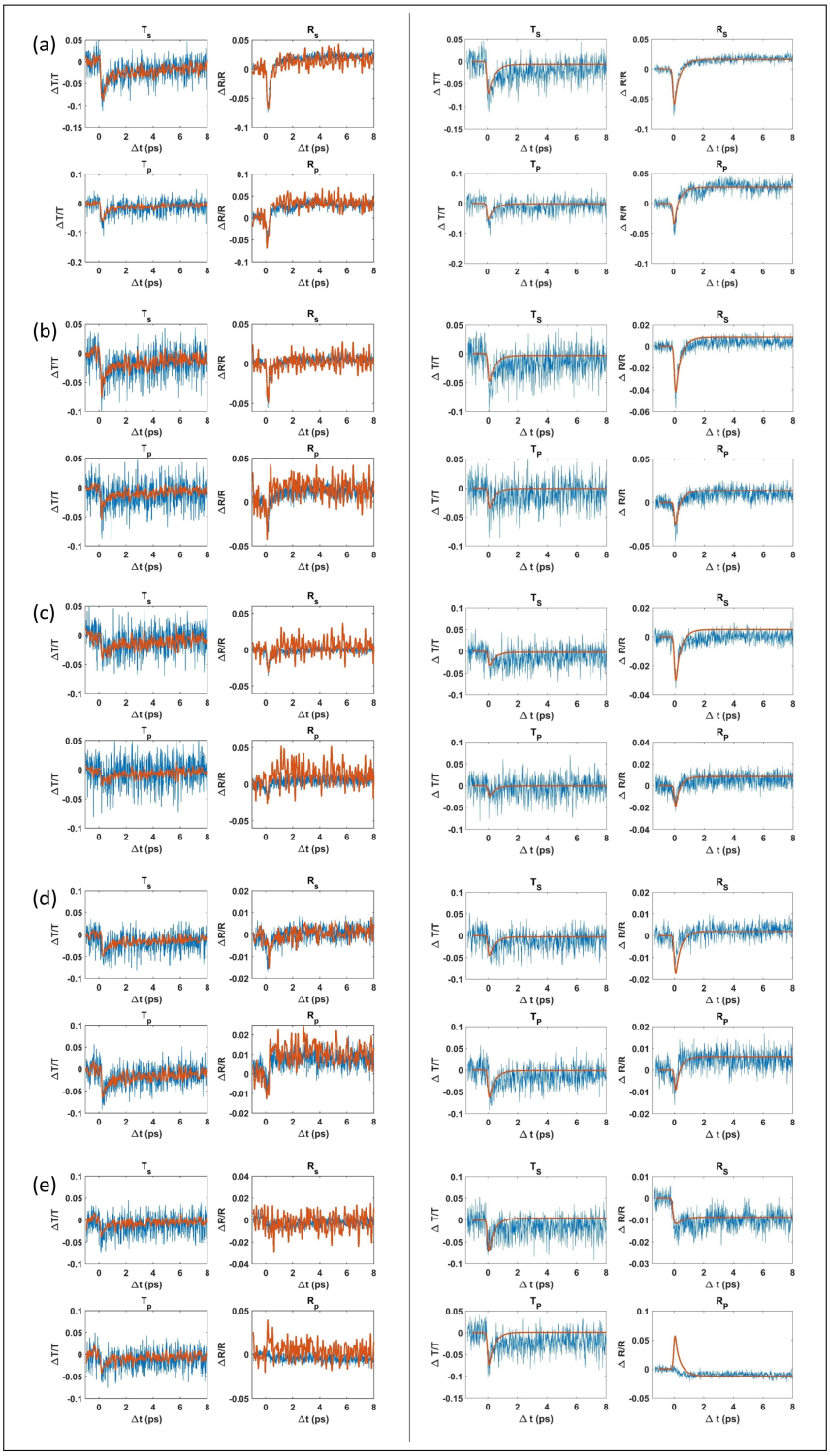

Fig. 7. S and P reflectivity and transmissivity traces (blue curves) acquired for the 38 nm (a-c), 110 nm (d), and 575 nm (e) membrane at 13 mJ/cm^2 (a, d, e), 7 mJ/cm^2 (b), and 4 mJ/cm^2 (c). The red curves are the retrieved data using Jones matrix formalism (left panel) and the data obtained with nTTM (right panel).

Optics EXPRESS

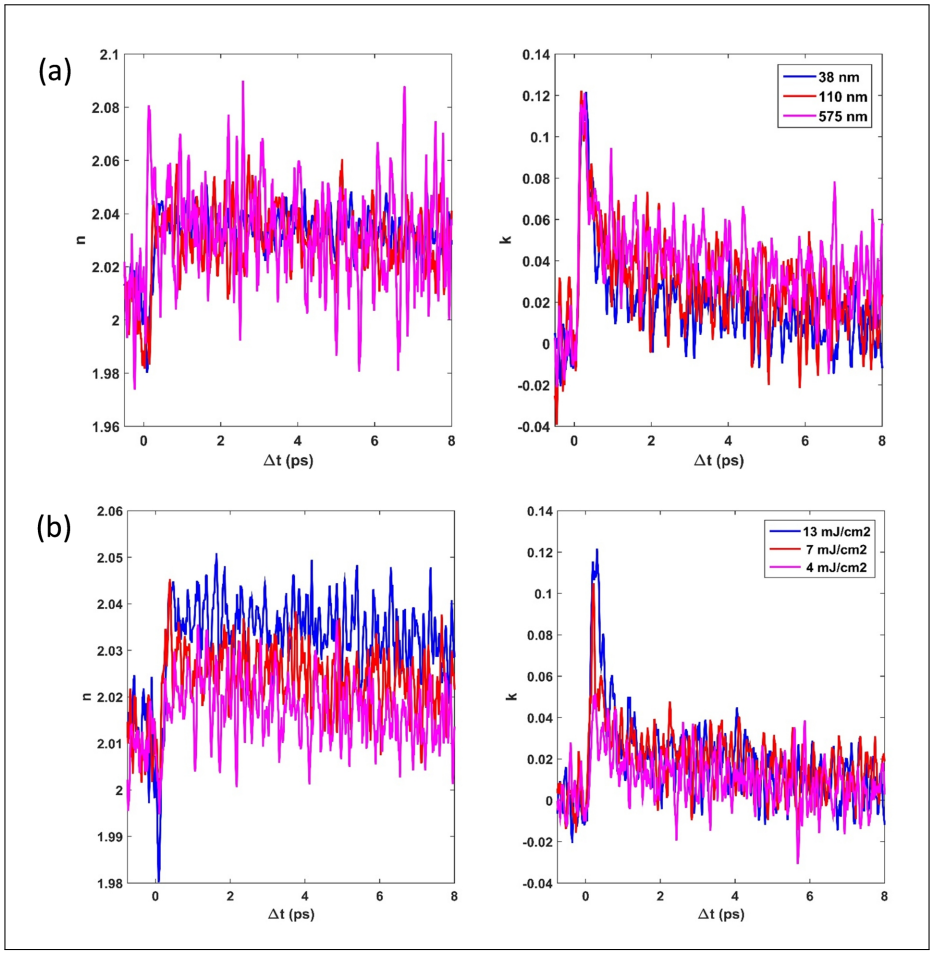

Fig. 8. The retrieved traces for n and k (for the first excited layer) obtained on 38 nm, 110 nm, and 575 nm thick membranes at 13 mJ/cm^2 FEL fluence (a), and 38 nm thick membrane only at 13, 7, and 4 mJ/cm^2 (b).